IEEE Access
Multidisciplinary | Rapid Review | Open Access Journal

Received 30 October 2023, accepted 4 November 2023, date of publication 13 November 2023,
date of current version 16 November 2023.

Digital Object Identifier 10.1109/ACCESS.2023.3332269

RESEARCH ARTICLE

Detection of Various Dental Conditions on Dental Panoramic Radiography Using Faster R-CNN

SHIH-LUN CHEN[1], (Member, IEEE), TSUNG-YI CHEN[2], (Member, IEEE), YI-CHENG MAO[3], SZU-YIN LIN[4], (Member, IEEE), YA-YUN HUANG[5], CHIUNG-AN CHEN[6], YUAN-JIN LIN[5], MIAN-HENG CHUANG[1], AND PATRICIA ANGELA R. ABU[7], (Member, IEEE)

[1]Department of Electronic Engineering, Chung Yuan Christian University, Taoyuan 320314, Taiwan
[2]Department of Electronic Engineering, Feng Chia University, Taichung 407102, Taiwan
[3]Department of General Dentistry, Chang Gung Memorial Hospital, Taoyuan 61363, Taiwan
[4]Department of Computer Science and Information Engineering, National Ilan University, Yilan 26047, Taiwan
[5]Department of Program on Semiconductor Manufacturing Technology, Academy of Innovative Semiconductor and Sustainable Manufacturing, National Cheng Kung University, Tainan 717005, Taiwan
[6]Department of Electrical Engineering, Ming Chi University of Technology, New Taipei 243303, Taiwan
[7]Department of Information Systems and Computer Science, Ateneo de Manila University, Quezon 1108, Philippines

Corresponding author: Szu-Yin Lin (szuyin@niu.edu.tw)

This work was supported in part by the National Science and Technology Council, Taiwan, under Grant 111-2221-E-033-041, Grant 111-2823-8-033-001, Grant 111-2622-E-131-001, Grant 110-2223-8-033-002, Grant 110-2221-E-027-044-MY3, Grant 110-2218-E-035-007, Grant 110-2622-E-131-002, Grant 109-2622-E-131-001-CC3, Grant 109-2221-E-131-025, Grant 109-2410-H-197-002-MY3, Grant 112-2410-H-197-002-MY2, and Grant 112-2222-E-035-004.

This work involved human subjects or animals in its research. Approval of all ethical and experimental procedures and protocols was granted by the Chang Gung Medical Foundation Institutional Review Board under Application No. 202002030B0.

ABSTRACT The dental panoramic radiograph (DPR) is a pivotal diagnostic tool in dentistry. However, despite the growing prevalence of artificial intelligence (AI) across various medical domains, manual methods remain the prevailing means of interpreting DPR images. This study aims to introduce an advanced identification system for detecting seven dental conditions in DPR images by utilizing Faster R-CNN. The primary objectives are to enhance dentists' efficiency and evaluate the performance of various CNN models as foundational training networks. This study contributes significantly to the field in several notable ways. Firstly, including a Butterworth filter in the training process yielded an approximately 7% enhancement in judgment accuracy. Secondly, the proposed enhancement technology tailored to different dental symptoms effectively bolstered the training model's accuracy. Consequently, all dental conditions attained an accuracy rate exceeding 95% in CNN analysis. These accuracy enhancements ranged from 1.34% to 13.24% compared to existing recognition technologies. Thirdly, this study pioneers the application of Faster R-CNN for identifying dental conditions, achieving an impressive accuracy rate of 94.18%. The outcomes of this study mark a substantial advancement compared to prior research and offer dentists a more efficient and convenient means of pre-diagnosing dental conditions.

INDEX TERMS Dental panoramic radiograph, database augmentation, image segmentation, image enhancement, CNN, Faster R-CNN.

I. INTRODUCTION

In recent years, with the development of medical technology, interdisciplinary research derived from precision medicine has become a hot project. Medical research has achieved good results in analyzing massive patient data through cross-disciplinary cooperation between researchers and doctors. Among them, the development of artificial intelligence is the most important. Artificial intelligence assistance systems are very significant in medicine [1]. These systems simplify the complex process of creating statistics and medical records. Moreover, the accuracy and execution efficiency of objective

The associate editor coordinating the review of this manuscript and approving it for publication was Yiming Tang.

data is improved. The topics of AI-assisted assistance in the medical field are diverse, including ventricular volume estimation, sleep stage classification, common tests during pregnancy, acute ischemic stroke lesions, prostate positioning, and glaucoma [2], [3], [4], [5], [6], [7].

Medical radiographs play an integral role in medical testing. Artificial intelligence also shines here. Excellent results have been achieved by combining various images such as computed tomography (CT) [8], magnetic resonance imaging (MRI) [9], ECG recognition [10], endoscopy image [11], and Orthopedics Radiographic [12], excellent results have been achieved. With the increasing attention to precision medicine topics, research topics related to dental health have also sprung up. The application of artificial intelligence to X-ray films commonly used in daily dentistry is also increasing, such as DPR [13], periapical radiograph [14], bitewing radiograph [15], and cone beam CT [16]. Before dental treatment, patients are often assisted in taking radiological images for diagnosis to provide dentists with a more effective diagnostic basis. Among them, DPR is a dental X-ray examination used for a preliminary understanding of the condition of the whole mouth. The entire oral cavity teeth, surrounding structures, and tissues are included in a single image. It has an important contribution to developing treatment plans, mainly in the early detection of suspected lesions for further preventive treatment and avoiding subsequent invasive treatment procedures [17], [18].

However, there is still room for improvement in the identification accuracy and efficiency of DPR in current dental research. In [19], [20], [21], and [22], DPR and CT images are used for training with good results. In this study, an automatic tooth classification technique utilizing an application was developed through transfer learning and image detection. Transfer learning by using image segmentation and preprocessing. Then use the training results to investigate the accuracy. For the final judgment, image preprocessing, such as image cropping [23], [24], feature extraction [25], [26], image filtering [27], and chiaroscuro [28], are effective in improving accuracy.

This research focuses on seven symptoms: stumps, implant teeth, missing teeth, patches, periodontal, impacted teeth, and root canals. The dental conditions and explanations are as shown in TABLE 1.

This study aims to enhance the accuracy of dental condition recognition by combining image processing techniques and training five different CNN models for each symptom. The five underlying networks, namely AlexNet, GoogLeNet, ResNet50, ResNet101, and VGG19, were employed to train the CNN models. The best-performing model is selected as the base model for Faster R-CNN through careful analysis and comparison. In this study, the Faster R-CNN model adopts AlexNet and GoogLeNet as the basic models for training, which can effectively reduce redundant feature extraction and improve recognition accuracy. The region of interest (ROI) is then mapped to the feature map, and the target region is detected using the unified dimension of ROI pooling. The contributions of this study are as follows:

TABLE 1. The dental conditions and explanations.

Dental condition	Explanation
Retained root	The crown is missing, and only the root remains, known as the retained root.
Implant	Tooth Restoration Technology to replace missing teeth with artificial teeth.
Missing	A condition where teeth are naturally missing, loose, or surgically removed.
Patches	Intraoral reconstruction is performed on the remaining tissue in the patient's mouth to treat patients with missing or severely damaged teeth.
Periodontal	The tissue around the tooth begins to become inflamed.
Impacted	An impacted tooth fails to erupt into the dental arch within the expected developmental window.
Root canal	A root canal is the naturally occurring anatomic space within the root of a tooth. It comprises the pulp chamber, the main canal(s), and more intricate anatomical branches.

1. The appearance of dental conditions is improved by adding a Butterworth filter to the image enhancement stage. In addition, the proposed method improves accuracy by nearly 7%.
2. The proposed system achieves a recognition accuracy rate of more than 95% for all seven types of dental conditions on CNN. Compared with existing recognition technology, the accuracy improvements range from 1.34% to 13.24%.
3. The combination with Faster R-CNN is proposed for the first time in dental condition recognition. The AlexNet and GoogLeNet-based object recognition models achieve an accuracy rate of 94.18%.
4. The proposed system can simultaneously identify and mark seven different types of dental conditions on DPR images, significantly reducing the workload for dentists.

This study collaborated with five professional dentists with more than three years of clinical experience to align with practical clinical applications. The Institutional Review Board (IRB) reviewed and approved the research protocol under number 202002030B0. The most crucial aspect of this study is to recognize various dental abnormalities through CNN and object detection models accurately and enhance model accuracy through image segmentation and image enhancement. Utilizing the proposed dental condition identification method provides more precise and objective judgment data for dentists and facilitates the advancement of precision medical technology.

The organization of this paper is as follows: Section II introduces the process of segmentation, positioning, and enhancement of DPR film. And describe the architecture of the CNN model and the process of combining Faster R-CNN. The findings are discussed in Section III. Finally, Section IV gives the conclusion and prospects.

II. METHODS

There are three stages involved in this study; the first stage is to use image processing techniques on DPRs to achieve image segmentation and image enhancement, the second stage is to accomplish transfer learning with CNN and learn from the results and accuracies of it, the third stage is to first label images then use the training result from the second stage as the base network for Faster R-CNN to train. Finally, the training results will be discussed and verified. The flowchart of the detection system in this study is shown in Fig. 1.

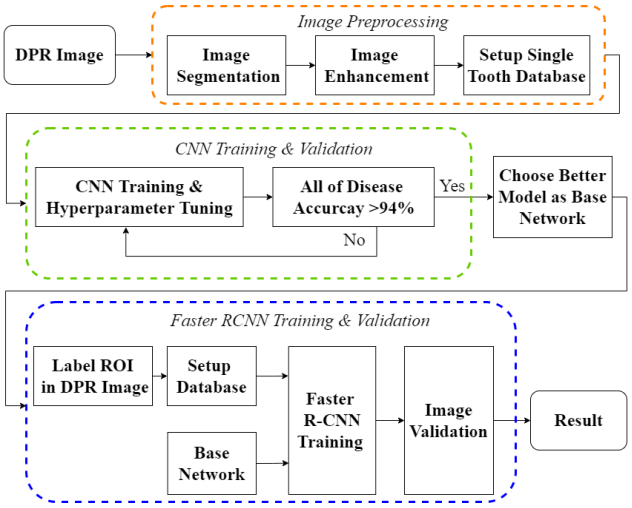

FIGURE 1. The flowchart of the detection system.

This study's two most important parts are image segmentation and CNN training. Image segmentation crops the image of a single tooth, thus reducing the interference caused by surrounding teeth. Helps to train the model more efficiently. In training the CNN, this research mainly focuses on applying the Faster R-CNN model and five different base networks to complete an object detection model for DPRs. Image preprocessing techniques are used first to highlight the possible lesion areas. Corresponding image enhancement is performed for different symptoms to obtain multiple image databases. Then use the best training result model as the base network of Faster R-CNN.

A. IMAGE PREPROCESSING

In the image preprocessing stage, the focus is on the pre-segmentation of single-tooth extraction. First, the DPR image is divided into upper and lower jaw parts. After that, image enhancements such as flat field correction, opening and closing operations, and image binarization are performed on the upper and lower jaw to find the gap. Then, the gap is used as the cutting point to complete the preprocessing of single-tooth segmentation. In Fig. 2, the flowchart of image preprocessing is displayed.

1) IMAGE SEGMENTATION

Many non-oral areas are present in an intact DPR membrane, as shown in Fig. 3. Additionally, the accuracy of the subsequently trained model is hampered by these non-oral regions. Experimenters discovered that multiplying the width of the original film by 0.61 and the length by 0.47 can remove the bone surrounding the teeth while leaving the teeth intact. The cropped image is shown in Fig. 4.

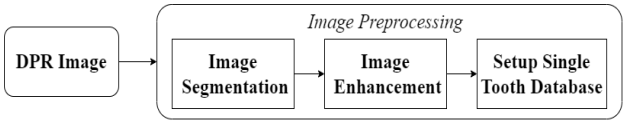

FIGURE 2. The flowchart of image preprocessing.

FIGURE 3. The original DPR images.

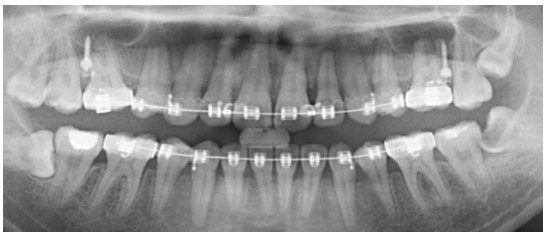

FIGURE 4. The DPR image after image segmentation.

2) IMAGE ENHANCEMENT

a: FLAT FIELD CORRECTION

Flat field correction is a technique for improving the quality of digital images [29]. Because people's mouth angles differ, image unevenness and cropping errors will occur when taking DPR images. The shadow component is approximated using Gaussian smoothing [28] with SIGMA standard deviation to even out all the images. To address the issue of uneven pixel values, a SIGMA value of 2 is set, and the outcome of the flat field correction is depicted in Fig. 5.

b: INTRANS ALGORITHM

There is a lot of noise in the original DPR image, which interferes with the cropping process and further impedes the output of a single-tooth image. As a result, in this study, the luminance variation function is used to perform the work of negative film conversion. The brightness change function is performed using the Intrans function after the image preprocessing steps in Fig. 6 are completed. The difference in

FIGURE 5. The image after the process of flat field correction.

(a)

(b)

FIGURE 6. Use the Intrans algorithm in the image preprocess phase (a) The image before Intrans procession. (b) The image after Intrans procession.

its input imagery is shown in Fig. 6 (b). The intrans function as Equation 1.

$$\frac{1}{1+(0.9*(\mathrm{Ia}+\mathrm{E})\text{^}4)} \tag{1}$$

The E represents an extremely small number that is about $2.2204e^{-16}$. Ia is the pointed pixel of the input image.

c: OPEN AND CLOSE OPERATION

Open and close operations are a type of spreading function used in morphology, and they use kernels to scan the original image when combined with the erode and dilate algorithm [31]. They are typically used to find the image's minimum and maximum areas. When the erode algorithm is used, it returns one if the results of all kernels scanning the image are all 1. Otherwise, it returns 0. If the results of all kernels scanning the image are all 0, the dilate algorithm will output 0. Otherwise, it will output 0. After the open operation goes through the erosion and dilation processes, certain things happen to the image, such as the image's silhouette being smoothed, the narrow parts being weakened and eliminated, the image being denoised, and the image being compressed, as shown in Equation 2. The close operation can assist in filtering out small holes or spots in the foreground object after it has gone through the dilation and erosion process depicted in Equation 3. A stands for the original film, and B stands for the kernels.

$$\mathrm{A} \circ \mathrm{B} = (\mathrm{A} - \mathrm{B}) \oplus \mathrm{B} \tag{2}$$

$$\mathrm{A} \bullet \mathrm{B} = (\mathrm{A} \oplus \mathrm{B}) - \mathrm{B} \tag{3}$$

In this study, the original image is subjected to open operation, after which it subtracts the pixel value of the original image and is referred to as IA. The same thing happens with the close operation known as IB. After that, add the original image with IA and subtract IB to obtain IC. Finally, ID can be obtained after undergoing another close operation with IC, as shown in Fig. 7.

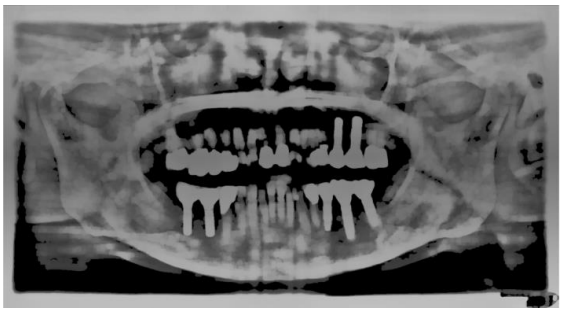

FIGURE 7. The result of the open and close operation.

d: OBTAIN THE SINGLE-TOOTH IMAGE

Efficient tooth separation is achieved by capturing interdental spaces, as elucidated in [30]. To mitigate the risk of gaps being overlooked, a hybrid approach involving interdental slit capture and the superimposition of a template, calibrated to the average tooth width, is employed to determine approximate boundary locations.

Leveraging the bilateral symmetry of the anterior tooth gap in both left and right jaw segments, this unique characteristic guides precise template positioning, facilitating seamless template superimposition onto radiographs. This alignment is executed by constraining the bite bar's downward detection range within the front teeth' confines. Upon identifying the jawbone's central point, the initial step involves the computation of the distance between the first reference point and the center point within the template and radiograph. Subsequently, these distances are designated as D1 for the template and D2 for the radiograph, with D1 preserving the proportional relationships between individual teeth, while D2 reflects the actual required distances. Finally, through a linear transformation, D2 is standardized to match the length of D1, thereby establishing the necessary framework for customizing the template to suit each radiograph.

e: BUTTER WORTH FILTER ALGORITHM

Image enhancement on single-tooth radiographs can significantly improve CNN training accuracy. The Butter Worth high-pass filtering [33] algorithm is the most important image enhancement technique in this study. This algorithm sharpens the image's edges to highlight the lesions, making it easier to identify the disease. Fig 8 depicts the results before and after image enhancement. Equation 4 represents the Butter Worth high-pass filtering algorithm.

$$H(u, v) = \frac{1}{1 + \frac{D_0}{D(u,v)}} \tag{4}$$

In Equation 4, D0 is the passband radius, and n is the number of Butterworth filters.

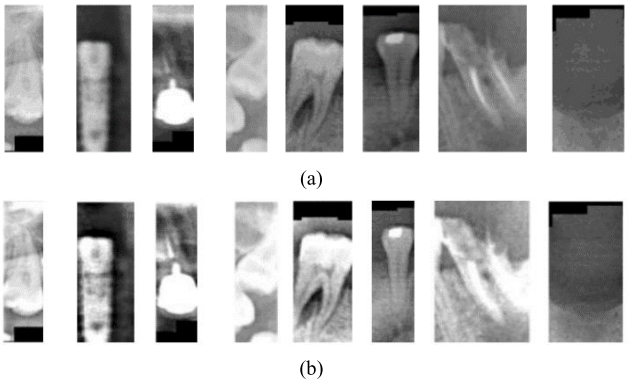

FIGURE 8. The single tooth images used in this study are, in order: original image, Implant, Root canal, Impacted, Periodontal, Patches, Retained root, and Missing teeth. The result of image enhancement (a) The original single-tooth image. (b) The result after the Butter Worth filter.

B. CNN TRAINING AND VALIDATION

A cognitive learning model that resembles the human brain is the convolutional neural network (CNN). When the symptoms of the disease are sufficiently similar, even experienced professionals in clinical imaging may misdiagnose the condition. A significant amount of image data can now be processed quickly and accurately by computer-aided medical imaging technology, which may subsequently be used to make accurate diagnoses and perform accurate segmentation and classification of various diseases. In this step, five CNNs are chosen to be trained. After the models' hyperparameters have been tweaked and the best training results have been obtained, two of the most appropriate models are selected as the Faster R-CNN base models. The flowchart of CNN training is shown in Fig. 9. TABLE 2 displays the hardware and software platforms used in this study's deep learning model training.

1) CNN MODEL ARCHITECTURE AND REVISION

This study employs five distinct CNN models: AlexNet, GoogLeNet, VGG19, ResNet50, and ResNet101. Take, for example, GoogLeNet, whose initial input has an image size of 224×224 × 3 pixels. However, in this study, the size of the input image is first fixed to 250 × 200 to approximate the original image ratio of 250 × 200×3. (RGB has three channels, and gray only has one channel).

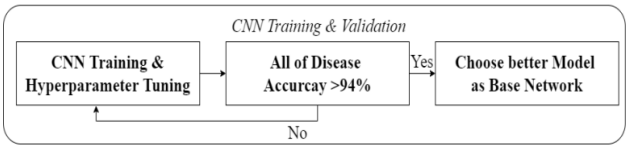

FIGURE 9. The flowchart of CNN training.

TABLE 2. The hardware and software platform.

Hardware platform	Version
CPU	AMD R5 3600X
GPU	GeForce RTX 2070 8G
DRAM	DDR4 2666 16G
Software platform	**Version**
MATLAB	R2021a
Deep Learning Toolbox	R2021a
Deep Network designer	14.2
Layer Library	14.2

TABLE 3. The GoogLeNet network architecture.

Type	Activation	Patch size / Stride
Image Input	250x200x3	
Convolution_1	125x100x64	7x7 / 2
Max Pooling_1	62x50x64	3x3 /2
Convolution_2	62x50x192	3x3 / 1
Max Pooling_2	31x25x192	3x3 /2
Inception (3a)	31x25x256	
Inception (3b)	31x25x480	
Max Pooling_3	15x12x480	3x3/2
Inception (4a)	15x12x512	
Inception (4b)	15x12x512	
Inception (4c)	15x12x512	
Inception (4d)	15x12x528	
Inception (4e)	15x12x832	
Max Pooling_4	7x6x832	3x3/2
Inception (5a)	7x6x832	
Inception (5b)	7x6x1024	
Global Average Pooling	1x1x1024	7x7/1
Dropout	1x1x1024	
Fully connect	1x1x8	
Softmax	1x1x8	

Moreover, GoogLeNet has an architecture different from other models, as shown in TABLE 3. Because it is difficult to predict when and how to apply Max-pooling and Convolution in most circumstances, GoogLeNet employs them all simultaneously to accomplish simplicity. It also outputs the Convolution of kernels of various sizes, as well as Max-pooling and Relu. Then, it concatenates into output, known as the Inception module, and the full GoogLeNet

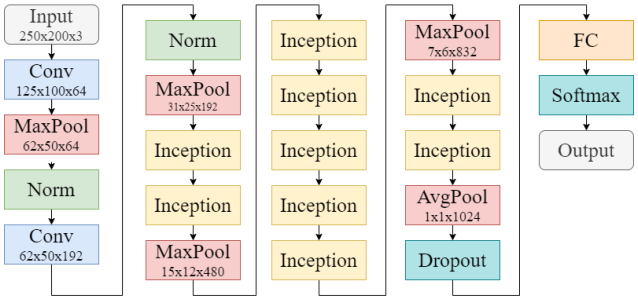

FIGURE 10. The GoogLeNet flowchart used in this study.

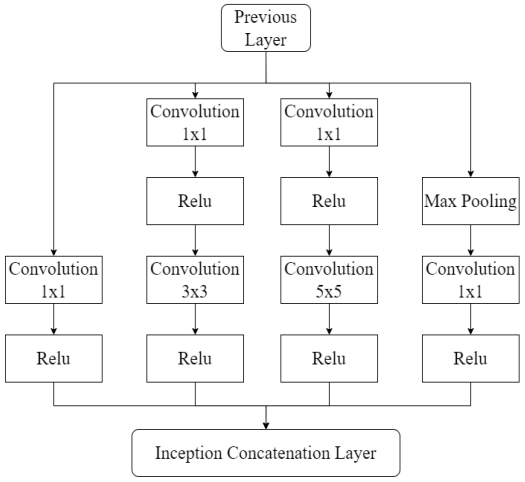

FIGURE 11. The inception module of GoogLeNet.

comprises multiple Inception modules. GoogLeNet is made up of 9 groups of inception modules, one of which is depicted in Fig. 10, and the flowchart of GoogLeNet is shown in Fig. 11. The Convolution block's N × N represents the filter size of each layer.

2) HYPERPARAMETER

The parameters and hyperparameters in this study train CNN and Faster R-CNN, which are readily confused. In general, parameters such as the weight w and deviation b of the Relu function are generated during training. Researchers, on the other hand, established hyperparameters after several trials. Deep learning hyperparameters such as initial learning rate, epoch, minibatch size, and the number of neurons in each layer are frequent. TABLE 4 shows three of the most critical hyperparameters found in this study.

TABLE 4. The HyperParameter value used in the deep learning.

	CNN	Faster R-CNN
Initial Learning Rate	1e-5	1e-3
MaxEpoch	100	50
Batchsize	32	4
Learning Rate Drop Factor	0.02	0.99
LearnRateDropPeriod	10	9
Shuffle	every-epoch	every-epoch

a: INITIAL LEARNING RATE

The initial learning rate determines the rate of gradient descent in the model, and if the Initial Learning Rate is set too low, the model converges slowly and is prone to overfitting. When the parameter is set too high, the model learns too quickly, cannot converge, fluctuates, and may even become divergent. The learning rate in this study decreased by 0.02% every ten epochs because the convergence rate is significantly slower by the late stage of training, and it may become trapped at the local minimum and fail to find the global optimal solution.

b: EPOCH

When all the photos have been calculated once, it produces one epoch. Because transferring the entire dataset once is insufficient, it should be done numerous times in the same neural network. As the number of epochs increases, so does the number of weights updating in the neural network, and the curve shifts from underfitting to overfitting. Multiple tests should be conducted to select an appropriate number of epochs for the dataset. In this study, CNN and Faster R-CNN are trained using 100 and 50 epochs, respectively.

c: MINIBATCHSIZE

The MiniBatchSize is the number of training samples gathered in a single training session. The batch size impacts how well and quickly the model is optimized. When the Hatch Size is too small, the model performs poorly, and the error rate increases dramatically. As the Batch Size grows, the same data will be processed faster. However, additional epochs are required to get the same level of accuracy. This study is conducted in CNN and Faster R-CNN, using training in 32 and 4 MiniBatchSize, respectively.

3) TRAINING AND VALIDATION

To monitor the learning progress of the model during training, this study divides the data, allocating eighty percent as the training dataset and the remaining twenty percent as the validation dataset, as depicted in TABLE 5. The validation set helps detect any overdependence on the training data, which can lead to inaccurate predictions on new data, often referred to as "overfitting." A key factor that leads to model overfitting is insufficient data. Therefore, this study augments the data by flipping the images horizontally and vertically, increasing the dataset by two to four times. Data augmentation technology only processes the data used to train the model and does not amplify the final predicted data. Its purpose is to increase the diversity and quantity of the training data by applying techniques such as rotation, flipping, and scaling, among others, which can create additional variations of the original data. Doing so can help prevent overfitting and improve the model's ability to generalize and make accurate predictions on new, unseen data. However, once the model is trained and deployed, data augmentation is no longer used,

and the predicted data is generated solely based on the learned model.

Finally, to ensure training accuracy, the numbers of suspected and asymptomatic cases in the training and validation sets were adjusted to maintain a consistent probability distribution that accurately predicts each class in a roughly 1:1 ratio. There are 350 images for each disease, and seven diseases are normal in total.

TABLE 5. Variation in the number of clinical images expected to be trained.

	Original	Augmentation
Implant	156	350
Root canal	124	350
Retained root	157	350
Periodontal	47	350
Patches	261	350
Impacted teeth	217	350
Missing	59	350
Normal	350	350

In this experiment, the model is not trained to identify the eight diseases; instead, it is trained to detect missing teeth before identifying the seven additional disorders on the remaining teeth (Implant, Root canal, Retained root, Periodontal, Patches, Impacted teeth, Normal). This research uses four distinct reference indicators for interpretation to verify whether the experimental data is correct after training, including accuracy, precision, recall, and the mAP. The calculating processes are shown in TABLE 6, and the formulas are as Equation (5)-(8).

$$\text{Accuracy} = \frac{\text{TP} + \text{TN}}{\text{TP} + \text{FP} + \text{TN} + \text{FNn}} \tag{5}$$

$$\text{Precision} = \frac{\text{Tp}}{\text{Tp} + \text{Fp}} \tag{6}$$

$$\text{Recall} = \frac{\text{Tp}}{\text{Tp} + \text{Fn}} \tag{7}$$

$$\text{mAP} = \frac{\sum_{q=1}^{Q} \frac{1}{n} \sum_{r\in\{0,0,1,\ldots.1\}} P_{\text{interp}}(q)}{Q} \tag{8}$$

C. FASTER RCNN TRAINING AND VALIDATION

Initially, DPR photos are annotated with disease names, and these images are subsequently incorporated into a database. Next, the elementary models chosen in the preceding stage are employed for training and testing within the Faster R-CNN framework. In Fig. 12, the flowchart depicting the training process of Faster R-CNN is presented. The K-fold cross-validation technique randomly partitions dataset A into k subsets, with one of the subsets designated as the test set in each iteration. In contrast, the remaining k-1 subsets are employed as the training set for model training. This study's dataset comprising 2800 single-tooth images is divided into ten subsets, facilitating testing in cases of limited sample size. The validation results reveal a correct rate of 98%.

Figure 13 illustrates the Faster R-CNN algorithm applied in this research. The Faster Region-based Convolutional

TABLE 6. Confusion matrix in two dimensions.

		Real	
		Positive	Negative
Predicted	Positive	TP (True Positive)	FP (False Positive)
	Negative	FN (False Negative)	TN (True Negative)

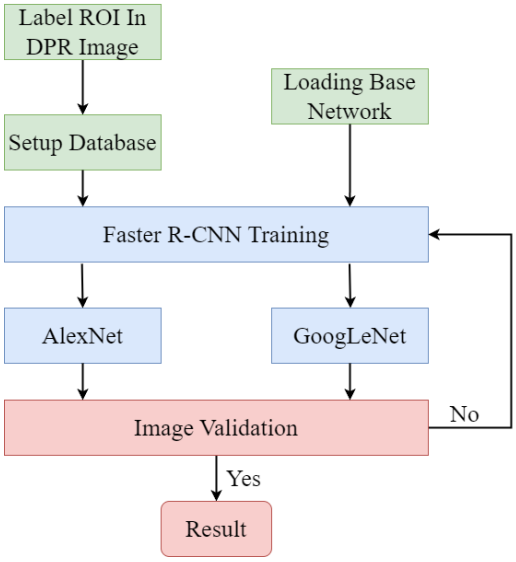

FIGURE 12. The flowchart of faster R-CNN training.

Neural Network (Faster R-CNN) algorithm is utilized to automate the detection of diverse dental conditions in circumoral radiographic images captured during panoramic X-ray examinations. This state-of-the-art computer vision model enhances the precision and efficiency of identifying dental conditions, consequently improving patient diagnosis and treatment planning.

1) IMAGE LABEL

The most significant aspect of this research is the region of interest (ROI), which may be defined using the simple Matlab Image Labeler and then used to label the ground truth data. The ground truth can be considered an absolute answer or a group of valid values. Ground truth is a sort of training data in machine learning that classifies supervised learning algorithms and is frequently used in statistics to prove or refute hypotheses. In this study, a collection of frames is defined in each image, with the frame elements ranging from 1 to 8. The number of ROIs determines the number of frames required in the image, and the set of frames is referred to as ground truth. And the types of teeth marked here included seven different diseases. As shown in Fig. 14 and Fig. 15, each disease uses a different colored frame, such as a pink frame for the root canal, a light purple frame for missing teeth, a light green frame for patches, a dark green

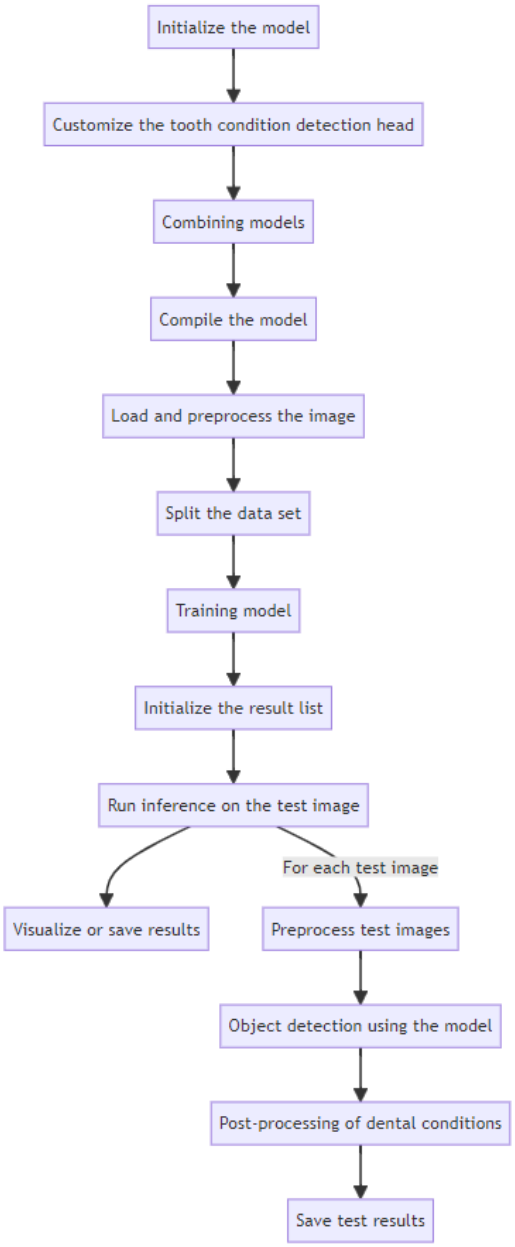

FIGURE 13. The flowchart of faster R-CNN training.

frame for implants, and a dark purple frame for periodontal disease.

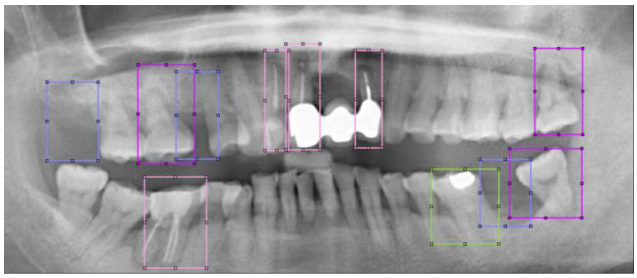

FIGURE 14. Image label for missing, root canal, patches, and periodontal disease.

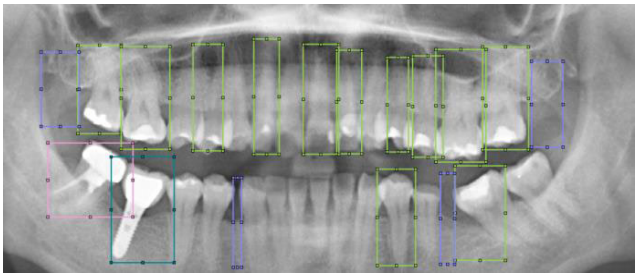

FIGURE 15. Image label for patches, missing, root canal, and implants.

2) FASTER R-CNN ARCHITECTURE

Object detection is a deep learning model that is used to detect objects. It is distinct from the Convolutional Neural Network (CNN), used mostly for classification. The Object detection model can recognize the positions of all objects of interest in an image and categorize them. Furthermore, it frames the objects with bounding boxes and calculates the corresponding confidence values. R-CNN, Fast R-CNN, Faster R-CNN, YOLO, SSD, and other models frequently generate object detection. CNN inspired the Faster R-CNN utilized in this study.

a: BASE NETWORK

A base network is the base model of the whole object detection model. In the hope of getting results faster and more efficiently, and because the training data is limited, transfer learning is used to obtain a set of pre-trained image classification networks. Transfer learning is a kind of deep learning that uses the existing model to solve similar problems. AlexNet and GoogLeNet, which both have high identification accuracy during the second stage, are used as the base models of Faster R-CNN.

b: REGION PROPOSAL NETWORK (RPN) NETWORK

The RPN architecture comprises several mini CNNs, anchors, and a regional proposal layer that functions as a candidate box to extract targets. The extraction procedure involves sliding different convolutional kernels on the DPR, producing a feature map, and selecting candidate regions using the anchor points. The RPN then computes the IoU values and classifies the predicted items as foreground or background based on the overlapping areas between the candidate regions and the actual bounding boxes. Finally, it returns the sizes and positions of the boxes and computes the loss. The IOU formula is shown in Equation 9.

$$IOU = \frac{A \bigcap B}{A \bigcup B} \tag{9}$$

The value of IoU denotes the overlapping area between the candidate region and the actual bounding box, with 0 representing no overlap and 1 representing complete overlap. The greater the value, the greater the overlap.

c: ANCHORS

An anchor box is a collection of preconfigured boxes used to identify individuals with a specific height and weight, with the size of the anchor box being almost identical to the subjects in the dataset. The position of an anchor box is established by repeatedly mapping the grid's output position to the input image. As a result, the entire image is covered in tiled anchor boxes. Each anchor box reflects a distinct class forecast. For example, two anchor boxes provide two predictions per place in Fig. 15.

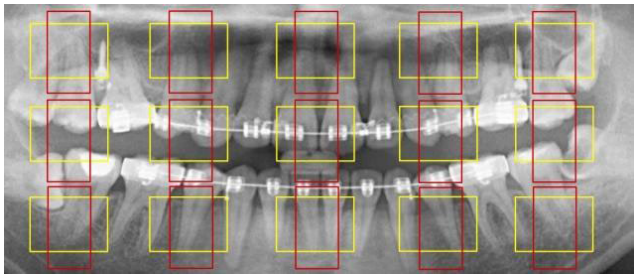

FIGURE 16. Two anchor boxes work at different positions on the image.

The detection framework sets anchor points of various sizes to accommodate objects of various sizes. In this study, five sizes of anchors were selected, the size of which is shown in TABLE 7, and one quality measure for judging the estimated anchor boxes is the mean IoU of the boxes in each cluster, and the overlap is calculated using a k-means clustering algorithm with the IoU distance metric. Equation 10 shows the k-means formula. The study will be more beneficial if the mean IOU can reach 0.8914.

$$J = \sum_{i=1}^{k} \sum_{xj} (xj - ui)^2 \tag{10}$$

TABLE 7. Five different anchor boxes.

	height	Width
1	104	35
2	87	14
3	95	29
4	91	17
5	101	25
Mean IOU	0.8914	

3) DATABASE AUGMENTATION

The data augmentation approach increases accuracy by randomly modifying the original data. Using the approach, it is feasible to increase the diversity of the training data without increasing the number of labeled training samples.

Two types of datasets are employed for training in this work. The first is the original database; the system cannot be thoroughly taught with just 75 photos available for training. Consequently, the second database increases performance by reversing the photos in different orientations, panning the pixel range to [−25 25], and enlarging the image size randomly. The maximum image size range is 1.1 times the original image, and if the anchor overlap rate is more than 0.25, the area beyond the border is clipped, and the brightness and saturation of the training image are randomly changed. The larger training database may be stretched to 300 photos, as shown in TABLE 8, and the database extension can effectively improve training outcomes.

TABLE 8. The number of image databases for faster R-CNN.

Quantity	Training image
Original quantity	75
Select quantity	300

III. RESULTS

A. CNN TRAINING RESULT

The accuracy of the CNN network is calculated in the image classification results based on the image annotation and the model assessment findings. Fig. 17 and Fig. 18 depict the training procedure and the classification accuracy of the seven illnesses. Five distinct CNNs are being trained in this research.

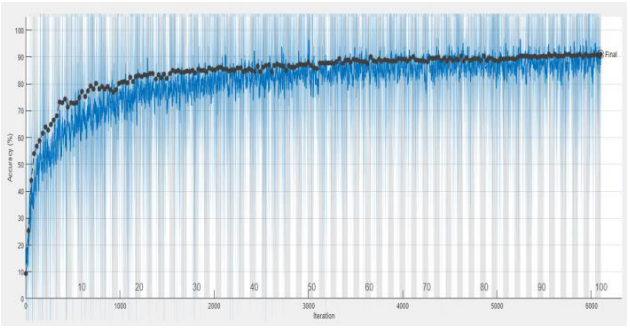

FIGURE 17. Accuracy training process of the GoogLeNet model in the training set (blue line) and the test set (black line).

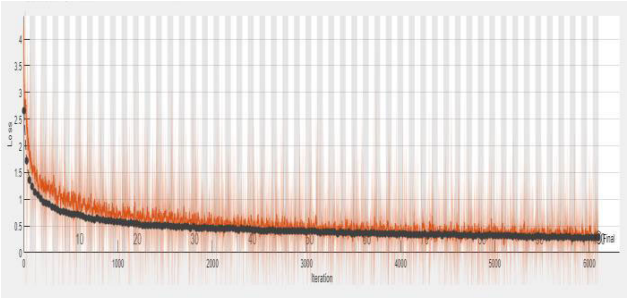

FIGURE 18. The loss function with the accuracy of the GoogLeNet model in the training set (orange line) and test set (black line).

During the missing teeth classification process, it is obvious that all models and accuracies are more than 95% before the image enhancement process, and the final accuracy may be as high as 99.81% after the process. The greatest increase, for example, is 4.07% for GoogLeNet.

And TABLE 9 displays the outcomes. After the missing teeth classification process, in terms of classifying the six illnesses and other teeth, the accuracy of each model is around 90% and 93% to 94% after applying the image improvement approach. The accuracy of the ResNet50 initially rises 4.74% from 88.54% after image improvement, then rises 1.62% to 95.81% following data augmentation, for a total gain of 7.27%. And

TABLE 10 displays the results. Finally, by performing horizontal and vertical image adjustments, random image rotation, and normal database augmentation procedures, the total result increases to 96%.

TABLE 9. Comparison before and after image enhancement for classification of missing teeth.

	Before	After Image Enhancement
AlexNet	98.61%	99.35%
GoogLeNet	95.74%	99.81%
ResNet50	97.89%	99.13%
ResNet101	96.50%	99.47%
VGG19	95.29%	98.38%

TABLE 10. Comparison before and after image enhancement and database augmentation in classifying six diseases and normal tooth.

	Before	After Image Enhancement	Image enhancement +Data augmentation
AlexNet	91.08%	94.92%	95.47%
GoogLeNet	89.59%	94.90%	96.52%
ResNet50	88.54%	93.28%	95.81%
ResNet101	90.66%	94.59%	96.64%
VGG19	87.91%	93.66%	94.08%

The identification accuracy of each illness was assessed, and the accuracy for each disease is presented in TABLE 11. The results indicate that the average recognition performance of each model exceeded 94.5%, which is a significant achievement. The high accuracy of the model in identifying different diseases is crucial for developing effective diagnosis and treatment plans. This is particularly important in medical imaging, where accurate diagnosis is vital to patient care and outcomes.

Identifying the symptoms of teeth is crucial at the CNN stage, and the dentists' DPR images are used for validation in this study to demonstrate the benefits of the practical application. The validation images and data are shown in Fig. 19, Fig. 20, and TABLE 12.

In Fig. 20, 32 teeth of the DPR image are labeled using the image segmentation technique and compared with the dentists' ground truth data in TABLE 12. In TABLE 12, GT represents the ground truth data; the ground truth refers to a benchmark value used to check whether the measurement data is reliable and is often used in deep learning. M stands for missing tooth, R stands for root canal, P stands for patch, I stands for implant, and O stands for other teeth. Almost

TABLE 11. The accuracies for different diseases after using the improved images.

	AlexNet	GoogLe Net	ResNet 50	ResNet 101	VGG19
Implants	99.89%	97.22%	97.25%	98.48%	92.21%
Root Canals	97.13%	98.45%	99.71%	97.21%	97.83%
Retained Root	97.09%	93.14%	96.13%	96.11%	94.07%
Periodontal	97.24%	92.95%	95.37%	96.31%	97.18%
Patches	82.75%	99.96%	95.20%	95.74%	94.59%
Impacted Teeth	99.98%	98.57%	94.66%	94.23%	97.75%
Missing	99.35%	99.81%	99.13%	99.47%	98.38%
Normal	91.93%	85.89%	92.77%	88.82%	86.46%
Average	95.67%	95.75%	96.28%	95.80%	94.81%

FIGURE 19. The DPR image for CNN model validation.

every tooth can be accurately classified into the correct disease, and all validation accuracies result above 95%.

TABLE 12. The validation result and ground truth comparison.

Label	18	17	16	15	14	13	12	11
GT	M	R	R	R	R	P	P	R
Validation	M	R	R	R	R	P	P	R
Accuracy	98%	97%	98%	99%	96%	94%	97%	97%
Label	21	22	23	24	25	26	27	28
GT	R	O	O	R	I	I	R	M
Validation	R	O	R	R	I	I	R	M
Accuracy	97%	92%	94%	96%	99%	99%	99%	97%
Label	31	32	33	34	35	36	37	38
GT	O	O	P	R	I	I	I	M
Validation	O	O	P	R	I	I	I	M
Accuracy	96%	97%	95%	98%	98%	99%	98%	98%
Label	48	47	46	45	44	43	42	41
GT	M	I	I	O	P	P	O	O
Validation	M	I	I	O	P	P	O	O
Accuracy	96%	98%	99%	91%	97%	96%	94%	96%

B. FASTER R-CNN TRAINING RESULT

The local segmentation procedure, illness labeling of the DPR image, and object identification model training are all part of this research step. Faster R-CNN networks are AlexNet and GoogLeNet, and the training process is depicted in Fig. 21.

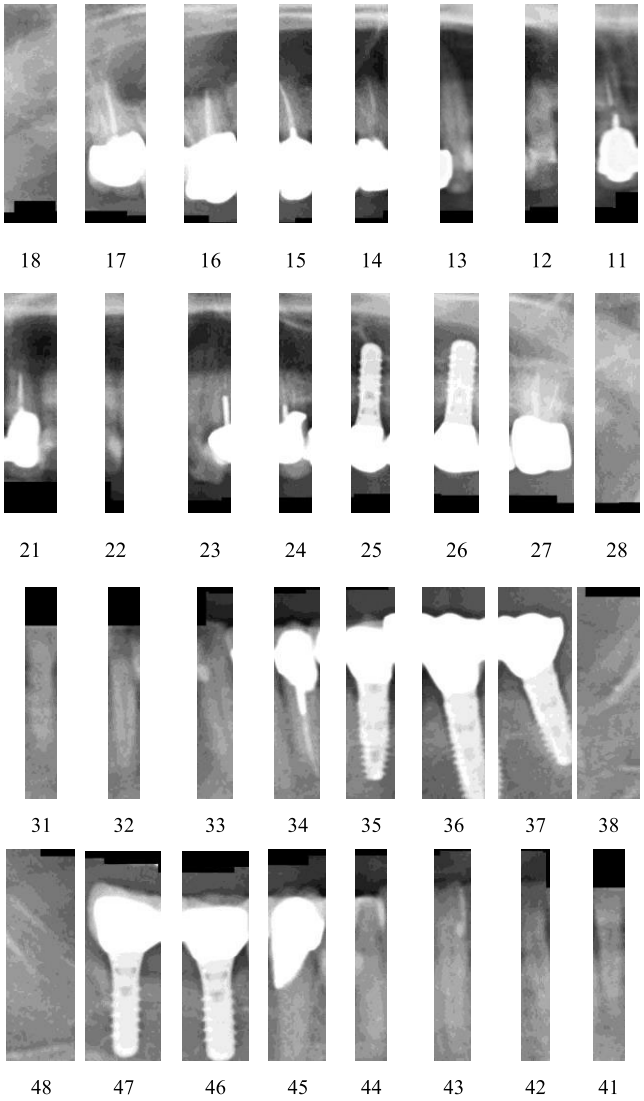

FIGURE 20. The split DPR image for validation and label number.

It may be stated that the applications of both networks are good in terms of object detection.

The training results and the accuracy rates are shown in TABLE 13. The accuracy rate of the network that uses GoogLeNet as the base network can be as high as 94.18%, and AlexNet also can reach 93.30%. The root-mean-square error (RMSE) value is approximately 0.12 in GoogLeNet and 0.14 in AlexNet. Both models' mean average precisions are more significant than 0.92.

This study also uses four YOLO-related models for analysis to further explore the distinctions between the more advanced YOLO technology and this study in terms of symptom identification. The experimental results are displayed in TABLE 14 for the four YOLO-related models: SSD-ResNet50, YOLOv2-DarkNet19, YOLOv4-Darknet53, and Yolov5s. The findings show that the training target detection model can reach 92.66% accuracy using YOLOv5s and 89.91% accuracy using SSD-ResNet50. Interestingly,

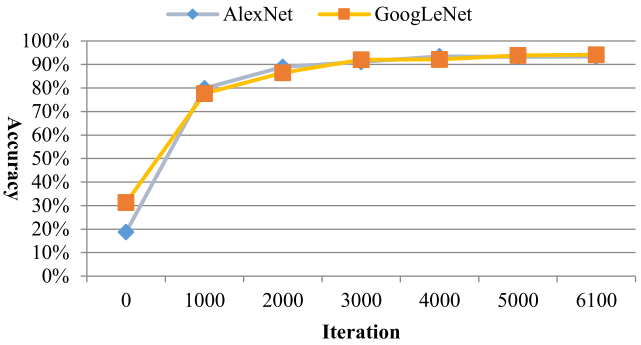

FIGURE 21. Comparison of the training process, the x-axis is iteration, and the y-axis is accuracy.

TABLE 13. Faster R-CNN training results using two different base networks.

Base Network	AlexNet	GoogLeNet
Accuracy	93.30%	94.18%
RMSE	0.14	0.12
Precision	94.88%	95.39%
Recall	93.19%	92.67%
mAP	0.9221	0.9315
Elapse Time	18:40	19:17

Faster R-CNN-GoogLeNet can achieve an accuracy rate of up to 94.18% with this technology, making this study roughly 1.52% more accurate than YOLOv5s.

TABLE 14. Comparison of training results using different object detection models.

Model	Accuracy	Precision	Recall
Faster R-CNN-GoogLeNet	94.18%	95.39%	92.67%
SSD-ResNet50	82.75%	73.39%	80.44%
YOLOv2 - DarkNet19	89.91%	86.32%	63.61%
YOLOv4 – DarkNet53	90.47%	91.28%	91.77%
Yolo v5s	92.66%	92.7%	93.46%

In addition, this study verifies the images in the folders that have not been used for training data and uses GoogLeNet as the base network. The results of image detection are shown in Fig. 22 and Fig. 23.

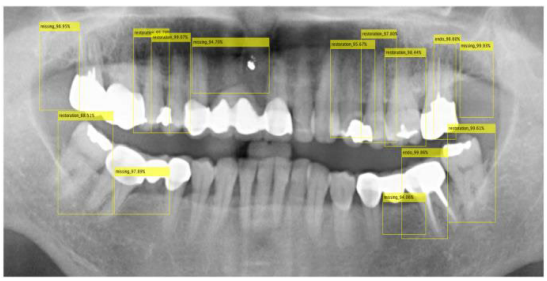

FIGURE 22. The first validation image.

This study compares the experiment's outcomes in the CNN training phase to the publications [34]. The accuracy rate in this investigation employing the single tooth image

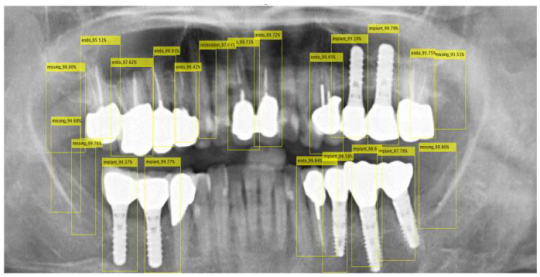

FIGURE 23. The second validation image.

database and the deep learning model of [34] may reach up to 83.28%, with a 13% difference between the trials, as shown in TABLE 15.

TABLE 15. Comparison of training results using CNN.

	Method in [34]	This Work
Accuracy	83.28%	**96.52%.**

While using the GoogLeNet as the base model, some modifications are done based on [35]. For example, unlike the CNN's input size from [35], the input size is changed from 227×227 to 250×200 in this study. The image enhancement approach from the study [35] can accomplish 95.18% when utilizing this study's single-tooth image database. However, the method used in this study can achieve 96.52%, resulting in a 1.44% difference between the studies. Furthermore, the accuracy in [36] that identifies six distinct implants may approach 95%, with a 1.52% difference between this study. Aside from that, the DPR images are used to train after being applied to the Butterworth filter. As a result of the adjustments, the recall of this research is up to 93.19%, which is 3.41% greater than the result from [36] and 20.25% greater than the result from [35].

Furthermore, this study's recall rate was as high as 93.19%. The improvement is up to 20% more than the [35] study's use of YOLO to determine the recall rate of 72.94%, and it is 3.41% higher recall than the [36]. This is an impressive advancement. The comparison of the results is presented in TABLE 16.

TABLE 16. Comparison of training results using CNN.

Comparison of training results using CNN			
	Method in [35]	Method in [36]	**This Work**
Accuracy	95.18%	95.00%	**96.52%.**
Recall	72.94%	89.78%	**93.19%**
mAP	0.6605	0.838	**0.9315**

IV. CONCLUSION

This study uses artificial intelligence (AI) to identify seven types of dental abnormalities on DPR images, including impacted, root canal, periodontal, retained root, endodontic treated teeth, missing, and implant, to alleviate the burden on dentists. The first stage involves training convolutional neural networks (CNNs), which employ two sets of training epochs, database augmentation, and the Butter Worth filter to enhance the identification of the seven diseases. These modifications can significantly improve validation accuracy, with GoogLeNet achieving a maximum accuracy of 96.52%. Compared to previous studies, this work has improved by 12%. This study adopts the Faster R-CNN model based on GoogLeNet and AlexNet in the second stage. The maximum accuracy rate of 94.18% is attained when GoogLeNet is used as the base network. Moving forward, this research will continue to improve the detection accuracy of Faster R-CNN and employ YOLO as the model to generate more efficient outcomes. This study significantly contributes to dental medicine by introducing an advanced AI-based system for identifying dental abnormalities on DPR images. The proposed system can enhance the efficiency of dentists and improve the accuracy of dental diagnoses, leading to better patient outcomes.

INSTITUTIONAL REVIEW BOARD STATEMENT

Chang Gung Medical Foundation Institutional Review Board; IRB number: 202002030B0; Date of Approval: 1 December 2020; Protocol Title: A Convolutional Neural Network Approach for Dental Bite-Wing, Panoramic and Periapical Radiographs Classification; Executing Institution: Chang Gung Medical Foundation Taoyuan Chang Gung Memorial Hospital of Taoyuan; Duration of Approval: From 1 December 2020 to 30 November 2021; The IRB reviewed and determined that it is expedited review according to Case research or cases treated or diagnosed by clinical routines. However, this does not include HIV-positive cases.

REFERENCES

[1] S. Niu, M. Liu, Y. Liu, J. Wang, and H. Song, "Distant domain transfer learning for medical imaging," *IEEE J. Biomed. Health Informat.*, vol. 25, no. 10, pp. 3784–3793, Oct. 2021, doi: 10.1109/JBHI.2021.3051470.

[2] S. Montaha, S. Azam, A. R. H. Rafid, M. Z. Hasan, A. Karim, and A. Islam, "TimeDistributed-CNN-LSTM: A hybrid approach combining CNN and LSTM to classify brain tumor on 3D MRI scans performing ablation study," *IEEE Access*, vol. 10, pp. 60039–60059, 2022, doi: 10.1109/ACCESS.2022.3179577.

[3] O. Daanouni, B. Cherradi, and A. Tmiri, "NSL-MHA-CNN: A novel CNN architecture for robust diabetic retinopathy prediction against adversarial attacks," *IEEE Access*, vol. 10, pp. 103987–103999, 2022, doi: 10.1109/ACCESS.2022.3210179.

[4] M. Han, H. Shim, and J. Baek, "Perceptual CT loss: Implementing CT image specific perceptual loss for CNN-based low-dose CT denoiser," *IEEE Access*, vol. 10, pp. 62412–62422, 2022, doi: 10.1109/ACCESS.2022.3182821.

[5] B. He, D. Xiao, Q. Hu, and F. Jia, "Automatic magnetic resonance image prostate segmentation based on adaptive feature learning probability boosting tree initialization and CNN-ASM refinement," *IEEE Access*, vol. 6, pp. 2005–2015, 2018, doi: 10.1109/ACCESS.2017.2781278.

[6] Y. Li, L. Zhang, H. Chen, and N. Yang, "Lung nodule detection with deep learning in 3D thoracic MR images," *IEEE Access*, vol. 7, pp. 37822–37832, 2019, doi: 10.1109/ACCESS.2019.2905574.

[7] Z. Khan, N. Yahya, K. Alsaih, S. S. A. Ali, and F. Meriaudeau, "Evaluation of deep neural networks for semantic segmentation of prostate in T2W MRI," *Sensors*, vol. 20, no. 11, p. 3183, Jun. 2020, doi: 10.3390/s20113183.

[8] Z. Huang, X. Liu, R. Wang, Z. Chen, Y. Yang, X. Liu, H. Zheng, D. Liang, and Z. Hu, "Learning a deep CNN denoising approach using anatomical prior information implemented with attention mechanism for low-dose CT imaging on clinical patient data from multiple anatomical sites," *IEEE J. Biomed. Health Informat.*, vol. 25, no. 9, pp. 3416–3427, Sep. 2021, doi: 10.1109/JBHI.2021.3061758.

[9] Z. Khan, N. Yahya, K. Alsaih, M. I. Al-Hiyali, and F. Meriaudeau, "Recent automatic segmentation algorithms of MRI prostate regions: A review," *IEEE Access*, vol. 9, pp. 97878–97905, 2021, doi: 10.1109/ACCESS.2021.3090825.

[10] L.-H. Wang, Y.-T. Yu, W. Liu, L. Xu, C.-X. Xie, T. Yang, I.-C. Kuo, X.-K. Wang, J. Gao, P.-C. Huang, S.-L. Chen, W.-Y. Chiang, and P. A. R. Abu, "Three-heartbeat multilead ECG recognition method for arrhythmia classification," *IEEE Access*, vol. 10, pp. 44046–44061, 2022, doi: 10.1109/ACCESS.2022.3169893.

[11] S. Wang, Y. Cong, H. Zhu, X. Chen, L. Qu, H. Fan, Q. Zhang, and M. Liu, "Multi-scale context-guided deep network for automated lesion segmentation with endoscopy images of gastrointestinal tract," *IEEE J. Biomed. Health Informat.*, vol. 25, no. 2, pp. 514–525, Feb. 2021, doi: 10.1109/JBHI.2020.2997760.

[12] Z. Liao, K. Liao, H. Shen, M. F. van Boxel, J. Prijs, R. L. Jaarsma, J. N. Doornberg, A. V. D. Hengel, and J. W. Verjans, "CNN attention guidance for improved orthopedics radiographic fracture classification," *IEEE J. Biomed. Health Informat.*, vol. 26, no. 7, pp. 3139–3150, Jul. 2022, doi: 10.1109/JBHI.2022.3152267.

[13] Y.-C. Huang, C.-A. Chen, T.-Y. Chen, H.-S. Chou, W.-C. Lin, T.-C. Li, J.-J. Yuan, S.-Y. Lin, C.-W. Li, S.-L. Chen, Y.-C. Mao, P. A. R. Abu, W.-Y. Chiang, and W.-S. Lo, "Tooth position determination by automatic cutting and marking of dental panoramic X-ray film in medical image processing," *Appl. Sci.*, vol. 11, no. 24, p. 11904, Dec. 2021, doi: 10.3390/app112411904.

[14] C.-W. Li, S.-Y. Lin, H.-S. Chou, T.-Y. Chen, Y.-A. Chen, S.-Y. Liu, Y.-L. Liu, C.-A. Chen, Y.-C. Huang, S.-L. Chen, Y.-C. Mao, P. A. R. Abu, W.-Y. Chiang, and W.-S. Lo, "Detection of dental apical lesions using CNNs on periapical radiograph," *Sensors*, vol. 21, no. 21, p. 7049, Oct. 2021, doi: 10.3390/s21217049.

[15] Y.-C. Mao, T.-Y. Chen, H.-S. Chou, S.-Y. Lin, S.-Y. Liu, Y.-A. Chen, Y.-L. Liu, C.-A. Chen, Y.-C. Huang, S.-L. Chen, C.-W. Li, P. A. R. Abu, and W.-Y. Chiang, "Caries and restoration detection using bitewing film based on transfer learning with CNNs," *Sensors*, vol. 21, no. 13, p. 4613, Jul. 2021, doi: 10.3390/s21134613.

[16] Z. Zheng, H. Yan, F. C. Setzer, K. J. Shi, M. Mupparapu, and J. Li, "Anatomically constrained deep learning for automating dental CBCT segmentation and lesion detection," *IEEE Trans. Autom. Sci. Eng.*, vol. 18, no. 2, pp. 603–614, Apr. 2021, doi: 10.1109/TASE.2020.3025871.

[17] M. G. Roberts, J. Graham, and H. Devlin, "Image texture in dental panoramic radiographs as a potential biomarker of osteoporosis," *IEEE Trans. Biomed. Eng.*, vol. 60, no. 9, pp. 2384–2392, Sep. 2013, doi: 10.1109/TBME.2013.2256908.

[18] A. Ajaz and D. Kathirvelu, "Dental biometrics: Computer aided human identification system using the dental panoramic radiographs," in *Proc. Int. Conf. Commun. Signal Process.*, Melmaruvathur, India, Apr. 2013, pp. 717–721, doi: 10.1109/iccsp.2013.6577149.

[19] R. Kaur, R. S. Sandhu, A. Gera, and T. Kaur, "Edge detection in digital panoramic dental radiograph using improved morphological gradient and MATLAB," in *Proc. Int. Conf. Smart Technol. For Smart Nation (SmartTechCon)*, Aug. 2017, pp. 793–797, doi: 10.1109/SmartTechCon.2017.8358481.

[20] A. K. Jain and H. Chen, "Matching of dental X-ray images for human identification," *Pattern Recognit.*, vol. 37, no. 7, pp. 1519–1532, Jul. 2004, doi: 10.1016/j.patcog.2003.12.016.

[21] R. Wanat and D. Frejlichowski, "A problem of automatic segmentation of digital dental panoramic X-ray images for forensic human identification," in *Proc. CESCG*, 2011, pp. 1–8.

[22] G. Jader, J. Fontineli, M. Ruiz, K. Abdalla, M. Pithon, and L. Oliveira, "Deep instance segmentation of teeth in panoramic X-ray images," in *Proc. 31st SIBGRAPI Conf. Graph., Patterns Images (SIBGRAPI)*, Oct. 2018, pp. 400–407, doi: 10.1109/SIBGRAPI.2018.00058.

[23] Y. Zhao, P. Li, C. Gao, Y. Liu, Q. Chen, F. Yang, and D. Meng, "TSASNet: Tooth segmentation on dental panoramic X-ray images by two-stage attention segmentation network," *Knowl.-Based Syst.*, vol. 206, Oct. 2020, Art. no. 106338, doi: 10.1016/j.knosys.2020.106338.

[24] X. Zhang, W. Pan, and P. Xiao, "In-vivo skin capacitive image classification using AlexNet convolution neural network," in *Proc. IEEE 3rd Int. Conf. Image, Vis. Comput. (ICIVC)*, Chongqing, China, Jun. 2018, pp. 439–443, doi: 10.1109/ICIVC.2018.8492860.

[25] B. M. Patil and B. Amarapur, "Segmentation of leaf images using greedy algorithm," in *Proc. Int. Conf. Energy, Commun., Data Analytics Soft Comput. (ICECDS)*, Aug. 2017, pp. 2137–2141, doi: 10.1109/ICECDS.2017.8389830.

[26] C.-C. Chang, J.-Y. Hsiao, and C.-P. Hsieh, "An adaptive median filter for image denoising," in *Proc. 2nd Int. Symp. Intell. Inf. Technol. Appl.*, Shanghai, China, Dec. 2008, pp. 346–350, doi: 10.1109/iita.2008.259.

[27] C.-C. Huang and M.-H. Nguyen, "X-ray enhancement based on component attenuation, contrast adjustment, and image fusion," *IEEE Trans. Image Process.*, vol. 28, no. 1, pp. 127–141, Jan. 2019, doi: 10.1109/TIP.2018.2865637.

[28] Z. Zhu, J. Li, L. Zhuo, and J. Zhang, "Extreme weather recognition using a novel fine-tuning strategy and optimized GoogLeNet," in *Proc. Int. Conf. Digit. Image Comput., Techn. Appl. (DICTA)*, Nov. 2017, pp. 1–7, doi: 10.1109/DICTA.2017.8227431.

[29] Y.-T. Peng, M.-H. Lin, C.-L. Tang, and C.-H. Wu, "Image denoising based on overlapped and adaptive Gaussian smoothing and convolutional refinement networks," in *Proc. IEEE Int. Symp. Multimedia (ISM)*, San Diego, CA, USA, Dec. 2019, p. 1363, doi: 10.1109/ISM46123.2019.00032.

[30] Y. Wang, Y. Gu, and X. Li, "A novel low rank smooth flat-field correction algorithm for hyperspectral microscopy imaging," *IEEE Trans. Med. Imag.*, vol. 41, no. 12, pp. 3862–3872, Dec. 2022, doi: 10.1109/TMI.2022.3198946.

[31] A. Yin, "Operators to dilate and erode color impulse noise images based on the morphology," in *Proc. Int. Conf. E-Business E-Government (ICEE)*, Shanghai, China, May 2011, pp. 1–3, doi: 10.1109/ICEBEG.2011.5882400.

[32] S.-L. Chen, T.-Y. Chen, Y.-C. Mao, S.-Y. Lin, Y.-Y. Huang, C.-A. Chen, Y.-J. Lin, Y.-M. Hsu, C.-A. Li, W.-Y. Chiang, K.-Y. Wong, and P. A. R. Abu, "Automated detection system based on convolution neural networks for retained root, endodontic treated teeth, and implant recognition on dental panoramic images," *IEEE Sensors J.*, vol. 22, no. 23, pp. 23293–23306, Dec. 2022, doi: 10.1109/JSEN.2022.3211981.

[33] S. RuoFei, "A design method of active high-pass butter-worth filter," in *Proc. IEEE Int. Workshop Electromagn., Appl. Student Innov. Competition (iWEM)*, Guangzhou, China, Nov. 2021, pp. 1–3, doi: 10.1109/iWEM53379.2021.9790408.

[34] N.-H. Lin, T.-L. Lin, X. Wang, W.-T. Kao, H.-W. Tseng, S.-L. Chen, Y.-S. Chiou, S.-Y. Lin, J. F. Villaverde, and Y.-F. Kuo, "Teeth detection algorithm and teeth condition classification based on convolutional neural networks for dental panoramic radiographs," *J. Med. Imag. Health Informat.*, vol. 8, no. 3, pp. 507–515, Mar. 2018, doi: 10.1166/jmihi.2018.2354.

[35] S.-Y. Lin and H.-Y. Chang, "Tooth numbering and condition recognition on dental panoramic radiograph images using CNNs," *IEEE Access*, vol. 9, pp. 166008–166026, 2021, doi: 10.1109/ACCESS.2021.3136026.

[36] B. Çelik and M. E. Çelik, "Automated detection of dental restorations using deep learning on panoramic radiographs," *Dentomaxillofacial Radiol.*, vol. 51, no. 8, Dec. 2022, Art. no. 20220244, doi: 10.1259/dmfr.20220244.

SHIH-LUN CHEN (Member, IEEE) received the B.S., M.S., and Ph.D. degrees in electrical engineering from National Cheng Kung University, Tainan, Taiwan, in 2002, 2004, and 2011, respectively. He was an Assistant Professor with the Department of Electronic Engineering, Chung Yuan Christian University, Taiwan, from 2011 to 2014, and an Associate Professor with the Department of Electronic Engineering, Chung Yuan Christian University, from 2014 to 2017, where he has been a Professor with the Department of Electronic Engineering, since 2017. His current research interests include VLSI chip design, image processing, wireless body sensor networks, the Internet of Things, wearable devices, data compression, fuzzy logic control, bio-medical signal processing, and reconfigurable architecture. He was a recipient of the Outstanding Teaching Award from Chung Yuan Christian University, in 2014 and 2019.

TSUNG-YI CHEN (Member, IEEE) received the B.S. and Ph.D. degrees in electrical engineering from Chung Yuan Christian University, Zhongli, Taoyuan, Taiwan, in 2020 and 2023, respectively. Since 2023, he has been an Assistant Professor with the Department of Electrical Engineering, Feng Chia University, Taiwan. His current research interests include VLSI chip design, image processing, internet of things, fuzzy logic control, wearable devices, machine learning, and biomedical signal processing.

YI-CHENG MAO was born in Taipei, Taiwan, in 1990. He received the bachelor's degree in dentistry from Chung Shan Medical University, Taichung, Taiwan, in 2015. He has been a resident who had operative dentistry specialist training with the Department of General Dentistry, Chang Gang Memorial Hospital, Taoyuan, Taiwan, since 2016. He received his operative dentistry specialist certificate from the Taiwan Academy of Operative Dentistry, in 2020. He has been an attending Doctor of General Dentistry, Taoyuan Chang Gang Memorial Hospital, since 2021.

SZU-YIN LIN (Member, IEEE) received the M.S. and Ph.D. degrees from National Chiao Tung University, Taiwan, in 2012. He was a Visiting Scholar with Coventry University, U.K., in 2012. In 2013, he was an Assistant Professor with the Department of Information Management, Chung Yuan Christian University (CYCU), Taiwan, where he was an Associate Professor, in 2017. In 2019, he was an Associate Professor with the Department of Computer Science and Information Engineering, National Ilan University (NIU), Taiwan. He has been a Professor with NIU, since 2022. His research interests include the areas of intelligent data analysis, artificial intelligence, machine learning, deep learning, management information systems, and service-oriented computing.

YA-YUN HUANG received the B.S. and M.S. degrees in electronic engineering from Chung Yuan Christian University, Zhongli, Taoyuan, Taiwan, in 2021 and 2023, respectively. She is currently working toward the Ph.D. degree with National Cheng Kung University, Tainan, Taiwan. Her current research interests include VLSI chip design, image processing, and image compression.

CHIUNG-AN CHEN received the B.S. degree in electronic engineering from Chung Yuan Christian University, Zhongli, Taoyuan, Taiwan, in 2005, and the Ph.D. degree in electrical engineering from National Cheng Kung University, Tainan, Taiwan, in 2013. Since 2017, she has been an Assistant Professor with the Department of Electrical Engineering, Ming Chi University of Technology, Taiwan. Her current research interests include VLSI chip design, image processing, wireless body sensor networks, the Internet of Things, wearable devices, biomedical signal, and image processing.

YUAN-JIN LIN received the B.S. degree in electronic engineering and computer science from Chung Yuan Christian University, Zhongli, Taoyuan, Taiwan, in 2023. He is currently pursuing the master's degree with National Cheng Kung University. His current research interests include VLSI chip design, image processing, and machine learning.

MIAN-HENG CHUANG received the B.S. degree in electronic engineering from Chung Yuan Christian University, Zhongli, Taoyuan, Taiwan, in 2021. She is currently pursuing the master's degree with Chung Yuan Christian University. Her current research interests include VLSI chip design, image cropping, and machine learning.

PATRICIA ANGELA R. ABU (Member, IEEE) received the B.S. degree in electronics and communications engineering from Ateneo de Manila University, Philippines, in 2007, the M.S. degree in electronics engineering major in microelectronics from Chung Yuan Christian University, Chung-Li, Taiwan, in 2009, and the Ph.D. degree in computer science from Ateneo de Manila University, in 2015. She is currently the Research Lab Head of the Ateneo Laboratory for Intelligent Visual Environments (ALIVE) and an Assistant Professor with the Department of Information Systems and Computer Science (DISCS), Ateneo de Manila University. Her current research interests include image processing and computer vision with applications that revolve on biomedical imaging and road/transportation, anomaly detection, and the IoT systems, which granted ALIVE several best research articles and presentation awards both local and abroad.